Supporting Information for
Anomalous collisions of elastic vector solitons in mechanical metamaterials

Bolei Deng[1], Vincent Tournat[1,2], Pai Wang[1], Katia Bertoldi[1, 3*]

[1]Harvard John A. Paulson School of Engineering and Applied Sciences
Harvard University, Cambridge, Massachusetts 02138, USA
[2]LAUM UMR CNRS, Le Mans Université, 72085 Le Mans, France
[3] Kavli Institute, Harvard University, Cambridge, Massachusetts 02138, USA

*To whom correspondence should be addressed; E-mail: bertoldi@seas.harvard.edu

November 7, 2018

S1 Fabrication

Our system is identical to that recently considered in (*1*) and consists of a long chain of 2×50 crosses made of LEGO bricks that are connected connected by thin and flexible hinges made of plastic shims. Each cross-shaped unit is realized using four brackets 2×2-2×2 (LEGO part 3956), as shown in Fig. S1. The hinges are realized by laser cutting the octagonal shape shown in Fig. S1A out of polyester plastic sheets (Artus Corporation, NJ - 0.005", Blue) with thickness $t_h = 0.127$ mm, Young's modulus $E = 4.33$ GPa and Poisson's ratio $\nu = 0.4$. The size of the octagonal shape is chosen to leave hinges of length $l_h = 4$ mm between the cross-shaped rigid units. Note that eight circular holes are incorporated into each hinge. They fit into the LEGO knobs and enable us to fix the hinges between the interlocking LEGO bricks (see

Fig. S1B). Note that in both samples identical bricks of different colors (black and gray) are used to facilitate visualization of the propagating pulses.

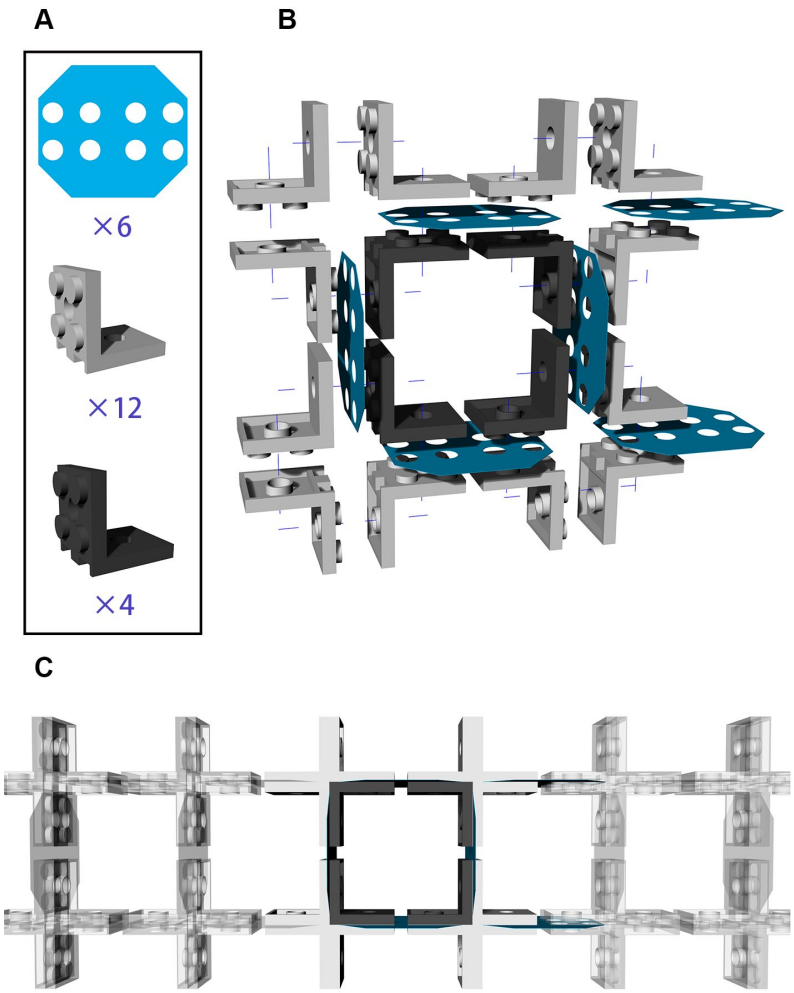

Figure S1: Fabrication of our structure. (A) Parts used to fabricate a 2×2 unit. (B) Exploded view of two pairs of crosses. (C) The chain is realized by putting together a number of 2×2 units.

S2 Testing

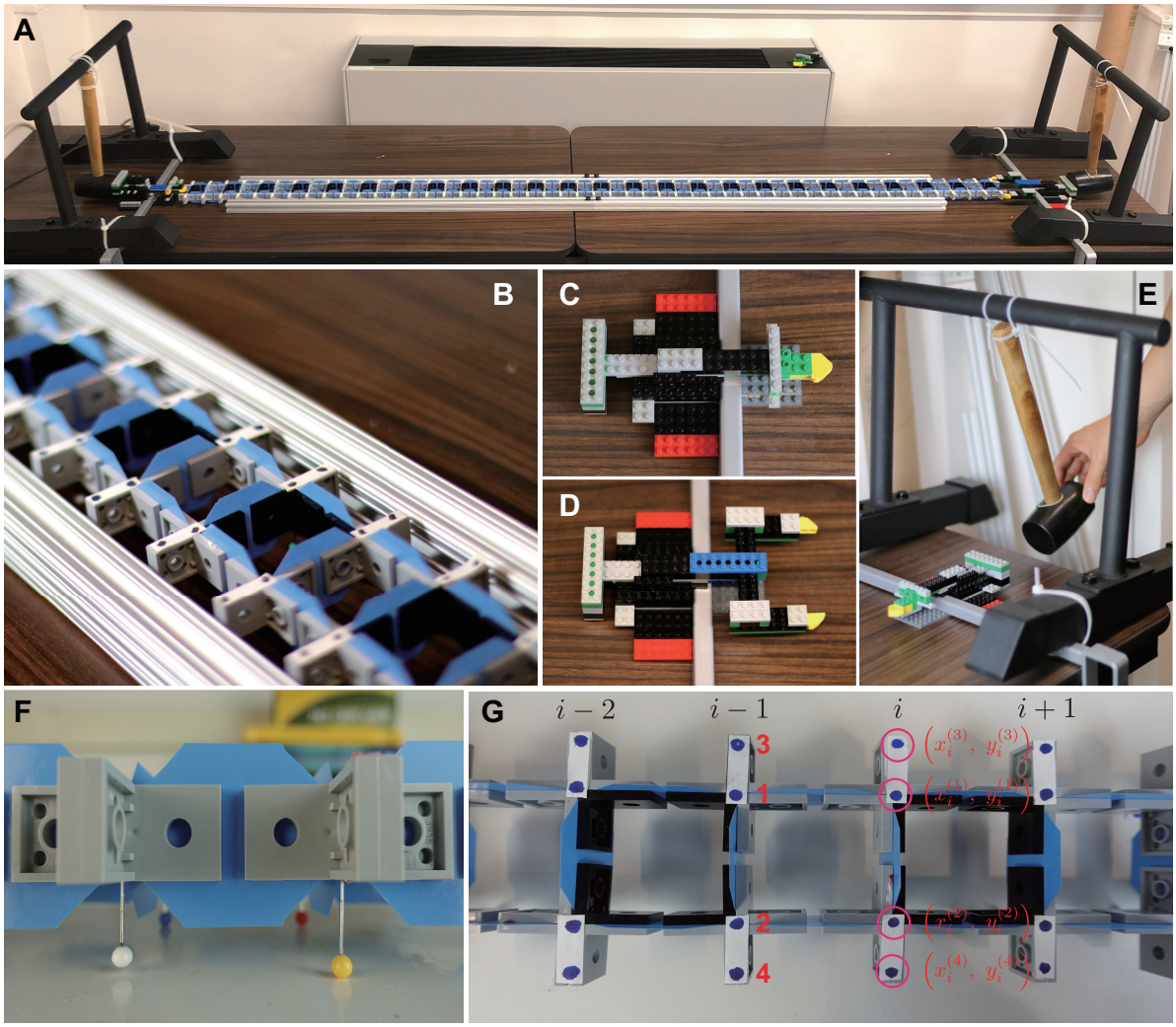

Figure S2: Experimental setup. (A) Pictures of our experimental setup showing the LEGO chain, the metal bars used to constrain the transverse movement of the chain and the pendulums and impactors used to excite the pulses at both ends. (B) A few units of our sample. (C) The impactor used to initiate solitons that excite positive rotations. (D) The impactor used to initiate solitons that excite negative rotations. (E) Close view of the pendulum consisting of a metal frame and a hammer. (F) Friction is minimized by supporting each rigid unit with pins. (G) Digital image correlation analysis. For each pair of rigid crosses four markers (blue dots) are tracked.

To investigate the propagation of pulses in our sample, we place the chain on a smooth horizontal surface (supported by pins to minimize the effect of friction - see S2F) and use two impactors excited by two pendulums (see Fig. S2A-B) to initiate the waves. Two metal bars are

placed on both sides of the chain to keep it straight. Note that the metal bars are not interacting with the chain during the propagation of nonlinear waves since the structure shrinks transversely due to the rotation of crosses. Different input signals are applied to the chain by varying both the strength of the pulse (controlled by the initial height of the striking pendulum) and the amplitude of the pulse (controlled by the distance traveled by the impactor). Furthermore, the direction of rotation imposed to the first and last pairs of crosses is controlled by using two different types of impactors. Specifically, since we define as positive a clockwise (counter-clockwise) rotation of the top unit in the even (odd) pairs, we use an impactor that hits the mid-point of the end pairs to excite positive rotation (see Fig. S2C) and one that hit their external arms to excite negative θ_i (see Fig. S2D). At this point we also want to point out that the direction of rotations imposed by the impactors changes if the chain comprises an odd number of pairs. If the chain has a odd number of pairs, the impactor that hits the mid-point of the last pair excite negative rotations (see Fig. S2C) and the one that hit the external arms of the last pair excite negative rotations (see Fig. S2D).

To monitor the displacement, u_i, and rotation, θ_i, of i-th pair of crosses along the chain as the pulses propagate, we use a high speed camera (SONY RX100V) recording at 480 fps and track four markers placed on the external arms of each pair of crosses (see S2G) via digital image correlation analysis (*2*). More specifically, the longitudinal displacement u_i and rotation θ_i of the i-th pair of rigid units is obtained as

$$\begin{aligned} u_i(t) &= \frac{1}{2} \sum_{\gamma=1,2} \left[x_i^{(\gamma)}(t) - x_i^{(\gamma)}(0) \right] \\ \theta_i(t) &= \frac{1}{2} \sum_{\gamma=1,2} (-1)^{i+\gamma} \arcsin \left[\frac{\left(x_i^{(\gamma+2)}(t) - x_i^{(\gamma+2)}(0) \right) - \left(x_i^{(\gamma)}(t) - x_i^{(\gamma)}(0) \right)}{\sqrt{\left(x_i^{(\gamma+2)}(0) - x_i^{(\gamma)}(0) \right)^2 + \left(y_i^{(\gamma+2)}(0) - y_i^{(\gamma)}(0) \right)^2}} \right] \end{aligned} \tag{S1}$$

where $\left(x_i^{(\gamma)}(t),\, y_i^{(\gamma)}(t) \right)$ and $\left(x_i^{(\gamma)}(0),\, y_i^{(\gamma)}(0) \right)$ are the coordinates of the γ-th marker placed on the i-th pair of rigid units at time t and that time $t = 0$ (i.e. before the impact), respectively.

S3 Mathematical Models

S3.1 Discrete model

Our system consists of a long chain of 2×N crosses with center-to-center distance a that are connected by thin and flexible hinges (see Fig. S3). Since in this work we focus on the propagation of longitudinal nonlinear waves along the chain, we assign two degrees of freedom to each rigid cross: the longitudinal displacement u and the rotation in the $x-y$ plane θ. Moreover, guided by our experiments, we assume that each pair of crosses shares the same displacement and rotates by the same amount, but in opposite directions (i.e. if the top cross rotates by a certain amount in clockwise direction, then the bottom one rotates by the same amount in counter-clockwise direction, and vice versa). As such, two degrees of freedom are assigned to the i-th pair of crosses: the longitudinal displacement u_i and the rotation θ_i (see Fig. S3). Moreover, to facilitate the analysis, we define a clockwise (counter-clockwise) rotation of the

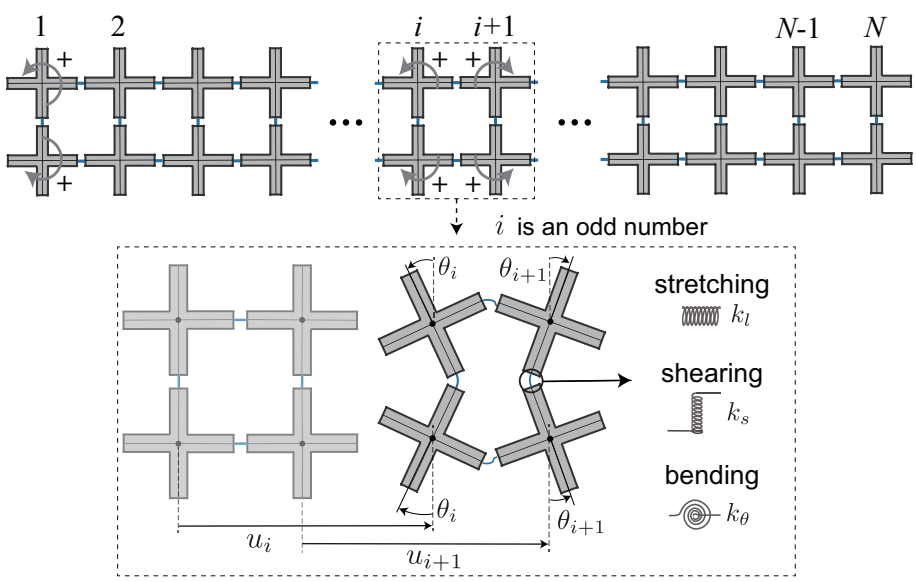

Figure S3: Schematics of the structure considered in this study.

top unit in the even (odd) columns to be positive, and similarly a clockwise (counter-clockwise) rotation of the bottom unit in the odd (even) columns to be negative (positive rotation directions

are denoted by yellow arrows in Fig. S3).

As for the hinges, we model them using a combination of three linear springs: (i) their stretching is captured by a spring with stiffness k_l; (ii) their shearing is governed by a spring with stiffness k_s; (iii) their bending is captured by a torsional spring with stiffness k_θ (see Fig. S3).

Under these assumptions, the equations of motion for the i-th pair of crosses are given by (*1*)

$$\begin{aligned} m\ddot{u}_i =& k_l \left[u_{i+1} - 2u_i + u_{i-1} - \frac{a}{2}\left(\cos\theta_{i+1} - \cos\theta_{i-1}\right)\right], \\ J\ddot{\theta}_i =& -k_\theta(\theta_{i+1} + 4\theta_i + \theta_{i-1}) + \frac{k_s a^2}{4}\cos\theta_i\big[\sin\theta_{i+1} - 2\sin\theta_i + \sin\theta_{i-1}\big] \\ & - \frac{k_l a}{2}\sin\theta_i\Big[(u_{i+1} - u_{i-1}) + \frac{a}{2}\big(4 - \cos\theta_{i+1} - 2\cos\theta_i - \cos\theta_{i-1}\big)\Big], \end{aligned} \tag{S2}$$

where m and J are the mass and moment of inertia of the rigid crosses, respectively.

Next, we introduce the normalized inertia $\alpha = a\sqrt{m/(4J)}$ and stiffness ratios $K_\theta = 4k_\theta/(k_l a^2)$ and $K_s = k_s/k_l$. Eqs. (S2) can then be written in dimensionless form as

$$\begin{aligned} \frac{a^2}{c_0^2}\frac{\partial^2 u_i}{\partial t^2} &= u_{i+1} - 2u_i + u_{i-1} - \frac{a}{2}\left[\cos\theta_{i+1} + \cos\theta_{i-1}\right], \\ \frac{a^2}{c_0^2\alpha^2}\frac{\partial^2 \theta_i}{\partial t^2} &= -K_\theta(\theta_{i+1} + 4\theta_i + \theta_{i-1}) + K_s\cos\theta_i\Big[\sin\theta_{i+1} + \sin\theta_{i-1} - 2\sin\theta_i\Big] \\ &\quad - \sin\theta_i\Big[2\left(u_{i+1} - u_{i-1}\right)/a + 4 - \cos\theta_{i+1} - 2\cos\theta_i - \cos\theta_{i-1}\Big], \end{aligned} \tag{S3}$$

where $c_0 = a\sqrt{k_l/m}$ is the velocity of the longitudinal linear waves supported by the chain in the long wavelength limit. As described in section S4, since it is extremely challenging to derive an analytical solution that captures the interaction between the solitons propagating in our system, we study collisions by numerically integrating the $2N$ coupled ordinary differential equations given by Eqs. (S3). Finally, we note that for the system considered in this study $K_s = 0.02$, $K_\theta = 1.5 \times 10^{-4}$ and $\alpha = 1.8$ (*1*).

S3.2 Analytical solution for a single pulse

Although it is extremely challenging to analytically describe the interactions between the pulses supported by our system, here we derive an analytical model to better characterize the propagation of a single wave. To this end, as recently shown in (*1*), we introduce two continuous functions $u\,(x,\,t)$ and $\theta\,(x,\,t)$ that interpolate the displacement and rotation of the i-th pair of crosses located at $x_i = ia$ as

$$u\,(x_i,\,t) = u_i(t), \quad \theta\,(x_i,\,t) = \theta_i(t). \tag{S4}$$

Assuming that the width of the propagating waves is much larger than the unit cell size, the displacement u and rotation θ in correspondence of the $i+1$ and $i-1$-th pairs of crosses can then be expressed using Taylor expansion as

$$\begin{aligned}
u_{i\pm1}(t) &= u\,(x_{i\pm1}, t) \approx u\Big|_{x_i,\,t} \pm a\frac{\partial u}{\partial x}\Big|_{x_i,\,t} + \frac{a^2}{2}\frac{\partial^2 u}{\partial x^2}\Big|_{x_i,\,t} \\
\theta_{i\pm1}(t) &= \theta\,(x_{i\pm1}, t) \approx \theta\Big|_{x_i,\,t} \pm a\frac{\partial \theta}{\partial x}\Big|_{x_i,\,t} + \frac{a^2}{2}\frac{\partial^2 \theta}{\partial x^2}\Big|_{x_i,\,t} \\
\cos\theta_{i\pm1}(t) &= \cos\left[\theta\,(x_{i\pm1}, t)\,\right] \approx \cos\theta\Big|_{x_i,\,t} \pm a\frac{\partial \cos\theta}{\partial x}\Big|_{x_i,\,t} + \frac{a^2}{2}\frac{\partial^2 \cos\theta}{\partial X^2}\Big|_{x_i,\,t} \\
\sin\theta_{i\pm1}(t) &= \sin\left[\theta\,(x_{i\pm1}, t)\,\right] \approx \sin\theta\Big|_{x_i,\,t} \pm a\frac{\partial \sin\theta}{\partial x}\Big|_{x_i,\,t} + \frac{a^2}{2}\frac{\partial^2 \sin\theta}{\partial x^2}\Big|_{x_i,\,t}
\end{aligned} \tag{S5}$$

Substitution of Eqs. (S5) into Eqs. (S3) yields

$$\begin{aligned}
\frac{1}{c_0^2}\frac{\partial^2 u}{\partial t^2} &= \frac{\partial^2 u}{\partial x^2} - \frac{\partial \cos\theta}{\partial x}, \\
\frac{a^2}{c_0^2\alpha^2}\frac{\partial^2 \theta}{\partial t^2} &= -a^2 K_\theta \frac{\partial^2 \theta}{\partial x^2} + a^2 K_s \cos\theta \frac{\partial^2 \sin\theta}{\partial x^2} + a^2 \sin\theta \frac{\partial^2 \cos\theta}{\partial x^2} \\
&\quad - 6K_\theta\theta - 4\sin(\theta)\Big[\frac{\partial u}{\partial x} + 1 - \cos\theta\Big],
\end{aligned} \tag{S6}$$

which represent the continuum governing equations of the system. Since these two coupled partial differential equations cannot be solved analytically, guided by our experiments, we further

assume that $\theta \ll 1$, so that

$$\sin\theta \approx \theta - \frac{\theta^3}{6}, \text{ and } \cos\theta \approx 1 - \frac{\theta^2}{2}. \tag{S7}$$

By substituting Eqs. (S7) into Eqs. (S6) and retaining the nonlinear terms up to third order, we obtain

$$\begin{aligned} \frac{1}{c_0^2}\frac{\partial^2 u}{\partial t^2} &= \frac{\partial^2 u}{\partial x^2} + \theta\frac{\partial \theta}{\partial x}, \\ \frac{a^2}{c_0^2\alpha^2}\frac{\partial^2 \theta}{\partial t^2} &= a^2\left(K_s - K_\theta\right)\frac{\partial^2 \theta}{\partial x^2} - 4\left[\frac{3K_\theta}{2} + \frac{\partial u}{\partial x}\right]\theta - 2\theta^3, \end{aligned} \tag{S8}$$

Finally, we introduce the traveling wave coordinate $\zeta = x - ct$, c being the pulse velocity, so that Eqs. (S8) become

$$\begin{aligned} \frac{\partial^2 u}{\partial \zeta^2} &= -\frac{1}{1 - c^2/c_0^2}\,\theta\frac{\partial \theta}{\partial \zeta} \\ \beta^{-1}\frac{\partial^2 \theta}{\partial \zeta^2} &= 4\left[\frac{3K_\theta}{2} + \frac{\partial u}{\partial x}\right]\theta + 2\theta^3, \end{aligned} \tag{S9}$$

where

$$\beta = a^{-2}\left[K_s - K_\theta - \frac{c^2}{\alpha^2 c_0^2}\right]^{-1} \tag{S10}$$

By integrating Eq. (S9)$_1$ with respect to ζ we obtain,

$$\frac{\partial u}{\partial \zeta} = -\frac{1}{1 - c^2/c_0^2}\,\frac{\theta^2}{2} + C \tag{S11}$$

where C is the integration constant. Since in this study we focus on the propagation of waves with a finite temporal support and do not consider periodic waves, we require that

$$\left.\frac{\partial u}{\partial \zeta}\right|_{\zeta\to\infty} = 0, \tag{S12}$$

from which we obtain $C = 0$. Substitution of Eq. (S11) into Eq. (S9)$_2$ yields

$$\frac{\partial^2 \theta}{\partial \zeta^2} = C_1\theta + C_3\theta^3 \tag{S13}$$

with

$$C_1 = 6\beta K_\theta, \text{ and } C_3 = -\frac{2\beta c^2}{c_0^2 - c^2}. \tag{S14}$$

Eq. (S13) is the Klein-Gordon equation with cubic nonlinearities, which admits analytical solution in the form of

$$\theta\left(x,t\right) = A \text{ sech}\left(\frac{x-ct}{W}\right), \tag{S15}$$

where A, c and W denote the amplitude, speed and width of the pulses. Moreover, by substituting Eq. (S15) into Eq. (S13), the solution for the displacement is found as

$$u(x,t) = \begin{cases} \dfrac{aA^2W}{2(1-c^2/c_0^2)}\left[1 - \tanh\left(\dfrac{x-ct}{W}\right)\right], & \text{for } c > 0 \\ \dfrac{aA^2W}{2(1-c^2/c_0^2)}\left[-1 - \tanh\left(\dfrac{x-ct}{W}\right)\right], & \text{for } c < 0 \end{cases} \tag{S16}$$

since for $c > 0$ (i.e. for solitons propagating from left to right) $u(\zeta \to \infty) = 0$, whereas for $c < 0$ (i.e. for solitons propagating from right to left) $u(\zeta \to -\infty) = 0$. Eqs (S15)-(S16) reveal an important feature of our system: its ability to support an elastic vector soliton. In fact, in our nonlinear system two components one translational and one rotational are coupled together and co-propagate without distortion nor splitting.

Next, we determine the relation between A, c, W and the geometry of the system. To this end, we substitute the solution (S15) into Eq. (S13) and find that the latter is identically satisfied only if

$$c = \pm c_0\sqrt{\frac{6K_\theta}{A^2 + 6K_\theta}}, \tag{S17}$$

and

$$W = a\sqrt{\frac{\alpha^2(K_s - K_\theta) - 6K_\theta/(A^2 + 6K_\theta)}{6\alpha^2 K_\theta}}. \tag{S18}$$

Eqs. (S15)-(S16) define the elastic vector solitons that propagate in our system. However, the existence of such waves require that W and c are real numbers. Inspection of Eqs. (S17)

and (S18) reveals that this condition is satisfied only if

$$\mathcal{A}_{\text{upper}} > A > \mathcal{A}_{\text{lower}}, \quad \text{with } \mathcal{A}_{\text{upper}} = -\mathcal{A}_{\text{lower}} = \sqrt{\frac{6K_\theta}{\alpha^2(K_s - K_\theta)} - 6K_\theta}. \tag{S19}$$

Notably, Eq. (S19) defines an amplitude gap for solitons, since it indicates that solitary waves with $A \in [\mathcal{A}_{\text{lower}}, \mathcal{A}_{\text{upper}}]$ cannot propagate in our system. Note that for the specific structure used in this study, $\mathcal{A}_{\text{upper}} = 0.12$ and $\mathcal{A}_{\text{lower}} = -0.12$.

Finally, the displacement and rotation induced by the propagating elastic vector solitons at the i-th pair of crosses can be determined from Eqs. (S15)-(S16) as

$$\theta_i\,(t) = \theta(x = ia, t) = A \text{ sech}\left(\frac{ia - ct}{W}\right), \tag{S20}$$

and

$$u_i(t) = \begin{cases} \dfrac{aA^2W}{2(1 - c^2/c_0^2)}\left[1 - \tanh\left(\dfrac{ia - ct}{W}\right)\right], & \text{for } c > 0, \\ \dfrac{aA^2W}{2(1 - c^2/c_0^2)}\left[-1 - \tanh\left(\dfrac{ia - ct}{W}\right)\right], & \text{for } c < 0. \end{cases} \tag{S21}$$

Equivalence between Eq. (S13) and the modified Korteweg-de Vries equation At this point we want to emphasize that the modified Korteweg-de Vries (modified KdV) equation can be written into the continuous governing equation of our system (the Klein-Gordon equation with cubic non-linearity given in Eq. (S13)). Here is the general form of the modified KdV equation (*3*):

$$\frac{\partial\theta}{\partial t} + F_1\frac{\partial^3\theta}{\partial x^3} - F_2\theta^2\frac{\partial\theta}{\partial x} = 0, \tag{S22}$$

F_1 and F_2 being constants. To demonstrate such equivalence, we first rewrite Eq. (S22) in terms of travelling wave coordinate $\zeta = x - ct$, obtaining

$$-c\frac{\partial\theta}{\partial\zeta} + F_1\frac{\partial^3\theta}{\partial\zeta^3} - F_2\theta^2\frac{\partial\theta}{\partial\zeta} = 0, \tag{S23}$$

and then integrate Eq. (S23) with respect to ζ yields

$$-c\theta + F_1\frac{\partial^2\theta}{\partial\zeta^2} - F_2\theta^3 = 0, \tag{S24}$$

considering that the integration constant is zero. This last equation can be rewritten in the same form of Eq. (S13) with

$$C_1 = \frac{c}{F_1}, \text{ and } C_2 = \frac{F_2}{F_1} \tag{S25}$$

S4 Numerical simulations

Since it is extremely challenging to derive an analytical solution that captures the interaction between the solitons propagating in our system, to study the collisions between the pulses supported by our system we numerically integrate the $2N$ coupled ordinary differential equations given by Eqs. (S3) for a given set of initial and boundary conditions. Specifically, in our simulations we consider 500 pairs of crosses and use $K_s = 0.02$, $K_\theta = 1.5 \times 10^{-4}$ and $\alpha = 1.8$. We use the 4th order Runge-Kutta method (via the Matlab function ode45) to numerically solve Eqs. (S3) (the code implemented in MATLAB is available online) As initial conditions we set $u_i = 0$, $\theta_i = 0$, $\dot{u}_i = 0$, $\dot{\theta}_i = 0$ for all pairs of crosses. Moreover, to excite solitons, we simply apply the analytical solution given by Eqs. (S20) and (S21) to the first and last unit of the chain. More specifically, at the left end we impose

$$\begin{aligned} \theta_1(t) &= A_{\text{left}} \operatorname{sech}\left(\frac{-c_{\text{left}}(t-t_0)}{W_{\text{left}}}\right), \\ u_1(t) &= \frac{aA_{\text{left}}^2 W_{\text{left}}}{2(1-c_{\text{left}}^2/c_0^2)}\left[1-\tanh\left(\frac{-c_{\text{left}}(t-t_0)}{W_{\text{left}}}\right)\right] \end{aligned} \tag{S26}$$

where W_{left} is given by Eq. (S18) and c_{left} is the positive solution of Eq. (S17). Moreover, t_0 is a parameter introduced to to ensure that $\theta_1 \to 0$ and $u_1 \to 0$ at $t = 0$ (in all our simulations we use $t_0 = 0.1$ sec). Differently, at the right end (i.e. for $i = N$) we impose

$$\begin{aligned} \theta_N(t) &= A_{\text{right}} \operatorname{sech}\left(\frac{-c_{\text{right}}(t-t_0)}{W_{\text{right}}}\right), \\ u_N(t) &= \frac{aA_{\text{right}}^2 W_{\text{right}}}{2(1-c_{\text{right}}^2/c_0^2)}\left[-1-\tanh\left(\frac{-c_{\text{right}}(t-t_0)}{W_{\text{right}}}\right)\right] \end{aligned} \tag{S27}$$

where W_{right} is also determined by Eq. (S18) and c_{left} is the negative solution of Eq. (S17).

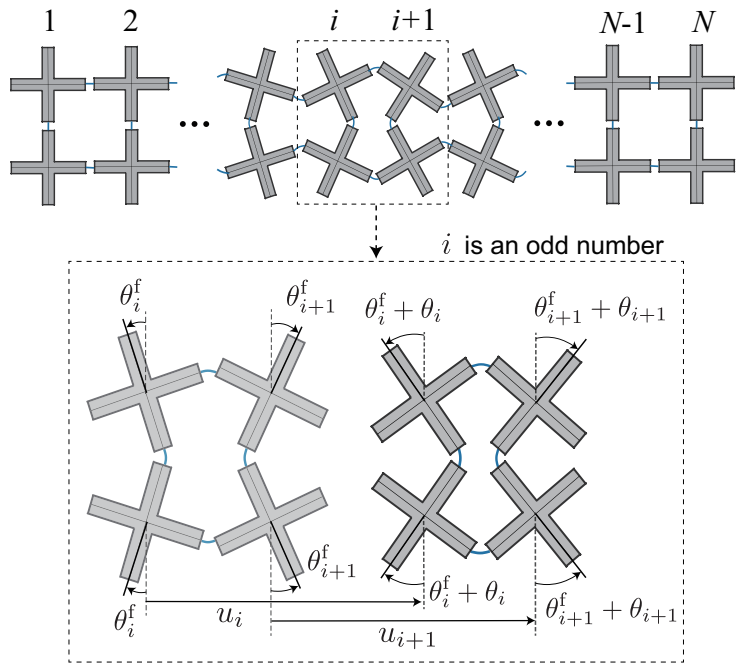

Figure S4: Schematics of the structure considered in this study with a frozen soliton located at its center.

As a part of this study we also consider frozen solitons of different amplitude A_{f} in the middle of the chain and numerically investigate their effect on the propagation of solitary waves initiated at the left end. In this case the discrete governing equations of the system (Eqs. (S3)) modify to

$$\begin{aligned}
\frac{a^2}{c_0^2}\frac{\partial^2 u_i}{\partial t^2} =& u_{i+1} - 2u_i + u_{i-1} - \frac{a}{2\cos\theta_i^{\mathrm{f}}}\left[\cos(\theta_{i+1}+\theta_{i+1}^{\mathrm{f}}) - \cos(\theta_{i-1}+\theta_{i-1}^{\mathrm{f}})\right],\\
\frac{a^2}{c_0^2\alpha^2}\frac{\partial^2 \theta_i}{\partial t^2} =& -K_\theta(\theta_{i+1}+4\theta_i+\theta_{i-1}) + K_s\cos(\theta_i+\theta_i^{\mathrm{f}})\Big[\sin(\theta_{i+1}+\theta_{i+1}^{\mathrm{f}})\\
&+\sin(\theta_{i-1}+\theta_{i-1}^{\mathrm{f}}) - 2\sin(\theta_i+\theta_i^{\mathrm{f}})\Big] - \sin(\theta_i+\theta_i^{\mathrm{f}})\Big[2\cos(\theta_i^{\mathrm{f}})\left(u_{i+1}-u_{i-1}\right)/a\\
&+4\cos(\theta_i^{\mathrm{f}}) - \cos(\theta_{i+1}+\theta_{i+1}^{\mathrm{f}}) - 2\cos(\theta_i+\theta_i^{\mathrm{f}}) - \cos(\theta_{i-1}+\theta_{i-1}^{\mathrm{f}})\Big].
\end{aligned} \tag{S28}$$

where θ_i^{f} is the initial rotation of the i-th pair of crosses due introduced because of the frozen pulse. For the specific case of a frozen soliton placed in middle of the chain,

$$\theta_i^{\mathrm{f}} = A_{\mathrm{f}}\,\mathrm{sech}\left[\frac{a\,(i-N/2)}{W_{\mathrm{f}}}\right], \tag{S29}$$

where A_{f} denotes the amplitude of frozen soliton and W_{f} is the width of the frozen soliton, which is determined by Eq. (S18) setting $A = A_{\mathrm{f}}$. As for boundary conditions, we apply input the theoretical solution at the left end as Eqs. (S26) and fixed boundary on the right end, i.e.,

$$\theta_N(t) = 0,\ u_N(t) = 0 \tag{S30}$$

Finally, we note that the numerical results for pulses characterized by $|A_{left}| < 0.12$ ($|A_{right}| < 0.12$) are obtained using Eqs. (S26) (Eqs. (S27)) with $W_{\text{left}} = 1$ ($W_{\text{right}} = 1$). This is because for $|A_{\text{left}}| < 0.12$ ($|A_{\text{right}}| < 0.12$) the width of the pulse given by Eq. (S18) is imaginary. Although this choice of width is arbitrary, quantitatively identical results are obtained for any real width (*1*).

S5 Additional results

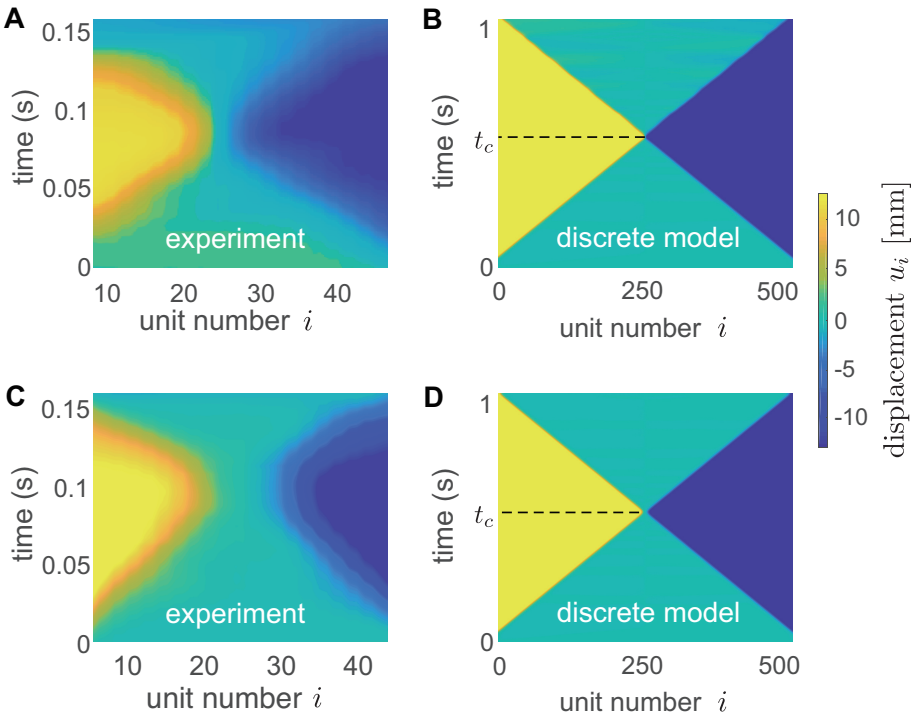

Figure S5: Displacement signal. (A)-(B) Longitudinal displacement of the pairs of crosses during the propagation of the pulses, as recorded in (A) experiments and (B) numerical simulations. The pulses excited at the left and right end are characterized by $A_{\text{left}} = 0.2$ and $A_{\text{right}} = 0.2$, respectively. (C)-(D) Longitudinal displacement of the pairs of crosses during the propagation of the pulses, as recorded in (C) experiments and (D) numerical simulations. The pulses excited at the left and right end are characterized by $A_{\text{left}} = -0.2$ and $A_{\text{right}} = 0.2$, respectively. In (C) and (D) we find that the units near collision point do not move - an indication of anomalous collisional dynamics.

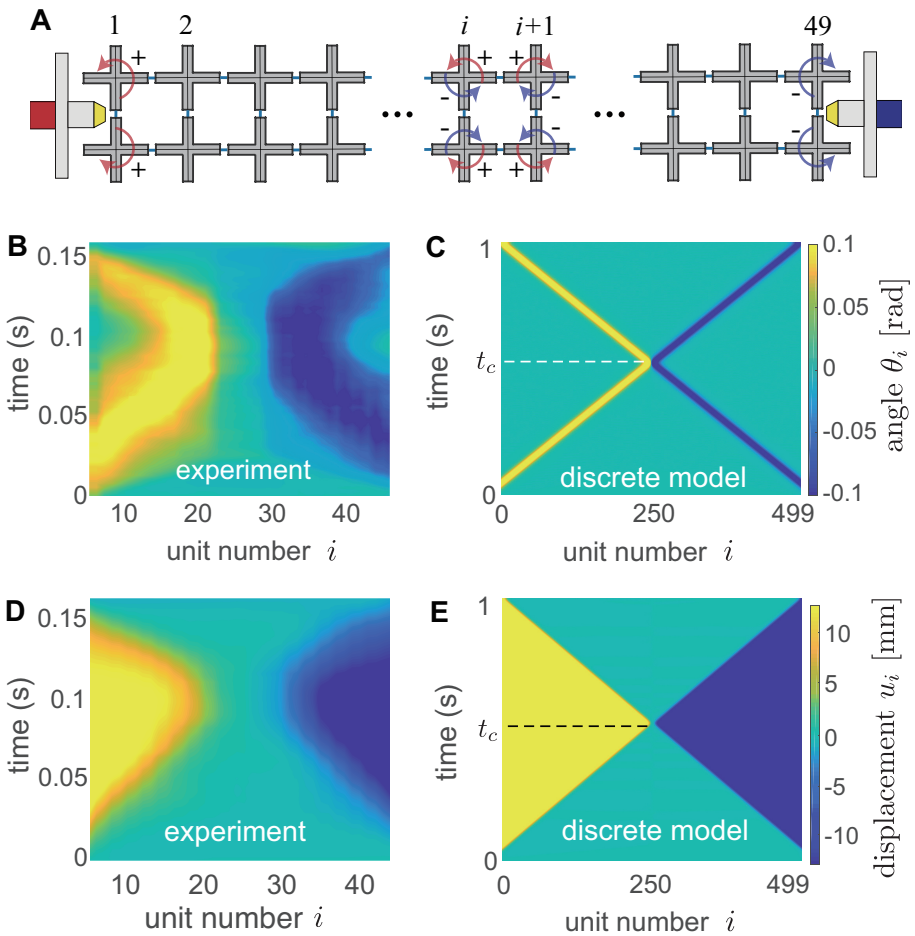

Figure S6: A chain with odd pairs of crosses. (A) We consider a chain with $N = 49$ pair of crosses. To initiate a solition at the right end that induces negative rotations, we use an impactor that hits the mid-point of the last pair. (B)-(C) Rotation of the pairs of crosses during the propagation of the pulses, as recorded in (B) experiments and (C) numerical simulations. (D)-(E) Longitudinal displacement of the pairs of crosses during the propagation of the pulses, as recorded in (D) experiments and (E) numerical simulations. The pulses excited at the left and right end are characterized by $A_{\text{left}} = 0.2$ and $A_{\text{right}} = -0.2$, respectively. The experiments are conducted on a chain with with 49 pairs of crosses, whereas in the numerical simulations we consider 499 units.

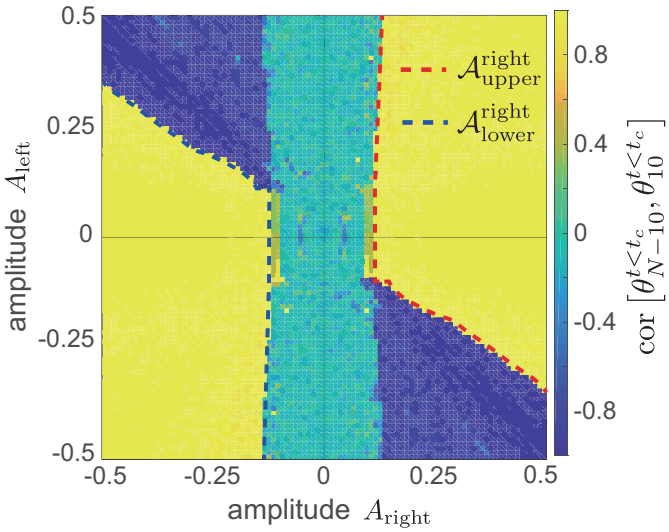

Figure S7: Numerically obtained cross-correlation between $\theta_{10}(t < t_c)$ and $\theta_{N-10}(t > t_c)$ as a function of A_{left} and A_{right}.

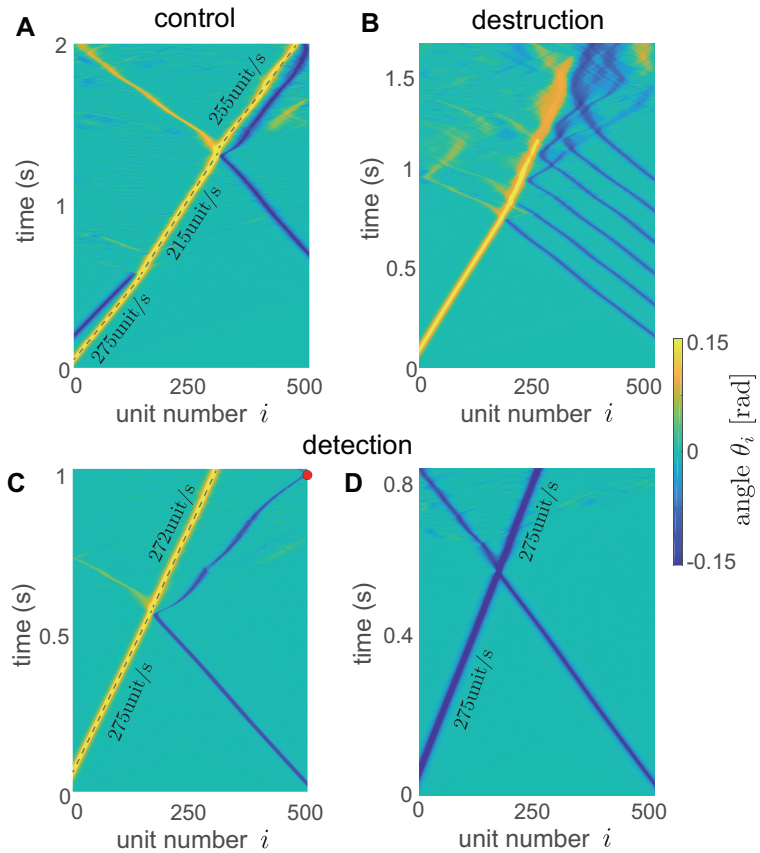

Figure S8: Anomalous collisions can be exploited to actively manipulate and control the propagation of pulses. (A) Anomalous collisions provide opportunities to remotely induce changes in the propagation velocity of a soliton. To demonstrate this, we consider a left-initiated pulse with $A_{\text{left},1} = 0.4$ and $c = 275$ unit/s and use the interactions with a soliton subsequently excited at the left end to reduce its velocity to $c = 215$ unit/s and with a right-initiated solitary wave to then accelerate it to $c = 255$ unit/s. (B) Anomalous collision can be exploited to block the propagation of a soliton. Specifically, a large propagating soliton can be blocked by sending a sequence of relatively small pulses with opposite rotation direction. As an example, we consider a left-initiated soliton with $A_{\text{left}} = 0.4$ and six right-initiated solitons with $A_{\text{right},k} = -0.2$ (with $k = 1, ..., 6$). Each of the six collisions results in energy radiation to linear waves or to other small amplitude solitons and reduces the amplitude of the left-initiated pulse, which eventually vanishes as its amplitude falls within the amplitude gap of the structure. Therefore, six small pulses efficiently mitigate and destroy the main left-initiated soliton at $t = 2$s. (C)-(D) Anomalous collisions can also be exploited to probe the direction of the rotational component of a pulse. To demonstrate this, we consider a main left-initiated soliton with $A_{\text{left}} = \pm 0.4$ and a probing, small right-initiated pulse with $A_{\text{right}} = -0.18$. If $A_{\text{left}} = 0.4$ (C), the "echo" of the probing soliton reaches the right end before the main soliton, indicating that it has been reflected by the main soliton. From this information, we therefore deduce that the main soliton is of positive amplitude. If $A_{\text{left}} = -0.4$ (D), no "echo" is observed, as the probe penetrate the main soliton. From this information, we therefore deduce that the main soliton is of negative amplitude. Finally, it is important to point out that, since the probing soliton carries much less energy than the main one, the latter is almost unaltered by the collision (i.e. its velocity changes from 275unit/s to 272unit/s).

References

1. B. Deng, P. Wang, Q. He, V. Tournat, K. Bertoldi, *Nature Communications* **9**, 3410 (2018).

2. M. Senn, *https://www.mathworks.com/matlabcentral/ fileexchange/50994-digital-image-correlation-and-tracking* (2016).

3. A. Polyanin, V. Zaitsev, *Handbook of Nonlinear Partial Differential Equations, Second Edition* (Chapman and Hall/CRC, 2011).